2ND CONFERENCE OF THE ARABIAN JOURNAL OF GEOSCIENCES (CAJG)
25-28 NOVEMBER 2019, SOUSSE, TUNISIA

Springer
SPRINGER NATURE

Tsunami hazard along the Eastern African coast from mega-earthquake sources in the Indian Ocean

Amir Salaree* **and Emile A. Okal**

Department of Earth & Planetary Sciences, Northwestern University, Evanston, IL 60208, USA

Arabian Journal of Geosciences

In preparation,
5 November 2019

* Present address: *Department of Earth & Environmental Sciences, University of Michigan, Ann Arbor, MI 48109, USA*

Abstract

The catastrophic 2004 Indonesian tsunami reached the shores of Eastern Africa, where it affected at least 12 countries and caused several hundred casualties, principally in Somalia. Significant variations in run-up were documented by various post-tsunami surveys (note that the latter remain incomplete, especially in Southern Tanzania and Mozambique). In a previous study, *Okal et al.* [2009] suggested that these variations could depend on the precise location of the tsunami sources, as a result of the combined effect of source directivity and refraction irregular bathymetry. In this context, we present the results of a significantly enhanced study, which considers a total of twelve potential sites of mega earthquakes, along both the Sunda Arc, and the Makran subduction zone. Numerical simulations are carried out at a total of 25 virtual gauges, spanning the East African coast from Socotra in the North to Port Elizabeth in the South, as well as adjoining islands (Madagascar, Comoros, Mascarenes). In particular, we identify locations where the 2004 tsunami (which to a large extent awakened the awareness of the continent to tsunami danger) may not have represented a worst case scenario.

1. Introduction and Background

The Sumatra-Andaman tsunami of 26 December 2004 was the first in modern history to export death and destruction acrossthe Indian Ocean Basin, resulting in more than 45,000 casualties in India and Sri Lanka alone. Farther out, it affected the coastlines of Eastern Africa, where it caused an additional ~300 casualties, principally in Somalia, but also all the way to South Africa where two people drowned at beaches near Port Elizabeth. In the following months and years, a number of extensive field surveys mapped run-up ranging up to 9 m in Somalia, 6.9 m in Grande Comore, and 5 m at the Southern tip of Madagascar [*Fritz and Borrero,* 2006, *Fritz and Okal*, 2008; *Okal et al.*, 2006*a,b,c*, 2009; *Weiss and Bahlburg*, 2006]; note however a significant gap in surveying from Southern Tanzania to Mozambique.

The 2004 disaster served as a tragic wake-up call to raise awareness of tsunami hazard among coastal populations of the Indian Ocean Basin, and in particular in East Africa. In its immediate wake, the Pacific Tsunami Warning Center in Hawaii and the Japan Meteorological Agency were given temporary responsibility for the issuance of warnings in the Indian Ocean [*Anonymous*, 2005], a function now transferred to regional outfits, following the development of adequate tsunami warning centers in a growing number of countries, including *e.g.,* Australia, Indonesia, India and Oman [*Bernard and Titov*, 2015].

In a previous study, *Okal et al.* [2009; hereafter Paper I] used numerical simulations to investigate a number of credible scenarios for future large Indonesian tsunamis impacting the Western Indian Ocean shorelines, and concluded that local effects

were responsible for significant lateral variations of run-up, which in turn meant that the 2004 event may not constitute a worst-case scenario at several locations along the coastlines of East Africa and its neighboring islands. In this context, we present here an update of the study in Paper I, which is enhanced in several respects. First, we increase the number of virtual gauges from 19 to 25, by targeting additional shorelines in Tanzania and Northern Mozambique (Figure 1); second, we fine-tune the position of all virtual gauges to ensure a commonality of water depth, chosen as 1000 m, for all locations, thus allowing more meaningful comparison between gauges. Finally, we add sources in the Makran subduction zone, the only other region with known earthquakes having generated large tsunamis in the

2. Hydrodynamic Simulations

2.1 Earthquake Sources

We use sources located at both the Sumatra and Makran Trenches, with all relevant parameters summarized in Table 1, which reproduces and expands a similar table in Paper I. Sumatra sources are identical to those used in Paper I. Source **S.I** models the 2004 event as a composite rupture. Source **S.II** uses *Okal and Synolakis*' [2008] model of the 1833 earthquake, based on the work of *Zachariasen et al.* [1999] and *Natawidjaja et al.* [2006]. Source **S.III** models the main 2007 Bengkulu earthquake, using *Borrero et al.*'s [2009] simple source. Source **S.IV** releases the strain left over on the 1797 and 1833 ruptures after the 2007 Bengkulu event, as detailed in *Okal and Synolakis* [2008]; it is representative of the widely expected Padang earthquake which should close that seismic gap in the next decades [*McCloskey et al.*, 2010]. Finally, Source **S.V** is similar to **S.IV**,

but extends South towards the Sunda Straits, and reproduces *Okal and Synolakis*' [2008] speculative Model 2*a*.

In the case of the Makran sources, we use the earthquake of 27 November 1945 as Source **M.B**. This event generated a devastating tsunami, with a large number of casualties in present-day Pakistan [*Pendse*, 1946]. Its mechanism and long-period moment are taken from *Okal et al.*'s [2015] inversion using the PDFM technique [*Reymond and Okal*, 2000]. Historical records [*Oldham*, 1893; *Ambraseys and Melville*, 1982] suggest the occurrence of tsunamigenic earthquakes on either side of the 1945 rupture, in 1851 (and possibly 1864) to the West, and in 1765 to the East. Following *Okal and Synolakis* [2008], we use such scenarios as models **M.A** and **M.C**, respectively. In the absence of detailed information about the source of these events, we assign them sizes and mechanisms similar to those of the 1945 shock (Model **M.B**), with the exception of the azimuth φ which we take as 281º in Model **M.A** in order to reflect the change in morphology of the coastline.

We then use the concept of fault fragmentation along a subduction zone to build three additional models in which two or more of the three blocks (A, B, C) rupture simultaneously. This concept, introduced by *Ando* [1975] in the case of the Nankai Trough, has later been confirmed in several other subduction systems, such as the Kuriles [*Nanayama et al.*, 2003], Cascadia [*Kelsey et al.*, 2005], or Southern Chile [*Cisternas et al.*, 2005]. Here, we consider Model **M.D** as a combined rupture of A and B, Model **M.E** as that of B and C, and finally Model M.F as the full rupture of all three segments A, B, and C.

Finally, we note that the exact tectonic regime of the Western part of the Makran subduction zone (West of source **M.A**) remains controversial. In the absence of firmly documented evidence for large scale seismicity, the convergence between Arabia and Eurasia (in excess of that taken up by onland orogeny) could be accommodated through either aseismic slip, or mega-thrust events recurring on a time scale of 1000 years or more so that none would be known in the available historical record [*Mokhtari et al.*, 2008; *Rajendran et al.*, 2013]. This situation is comparable to that which prevailed in Cascadia prior to the identification of the large 1700 earthquake [*White and Klitgord*, 1976]. Based on this remark, *Okal and Synolakis* [2008] considered the possibility of a mega-thrust scenario prolonging Model **M.F** ~450 km to the West (their Model 6), with a total moment 4.7×10^{29} dyn*cm, now comparable to that of the 2011 Tohoku earthquake. We incorporate this model as Scenario **M.G**, while stressing that it represents a very improbable situation combining several assumptions, all of which highly speculative: (i) that the Western Makran is a coupled subduction zone, when the only evidence of a major earthquake is a poorly constrained shock in 1483 [*Musson*, 2009]; (ii) that a single mega-event in the form of *Okal and Synolakis*' [2008] Model 6 could rupture the entire Makran coast, when the cross-cutting strike-slip Sonne Fault may interrupt the continuity of the subduction system [*Kukowski et al.*, 2000]; and (iii) that the slip on such a rupture would grow according to seismic similitude laws. That speculative nature will be emphasized when discussing our results.

2.2. Simulation Algorithm

Our simulations use the MOST algorithm [*Titov and Synolakis*, 1998; *Titov et al.*,

2016], which solves the full non-linear equations of hydrodynamics under the shallow-water approximation, by finite differences and using the method of alternate steps [*Godunov*, 1959]. MOST has been extensively validated through comparisons with laboratory and field data, per standard international protocols [*Synolakis et al.*, 2008]; full details can be found in *Synolakis* [2003].

As initial conditions for the vertical displacements of the sea surface, $\eta(t=0_+)$, we use the field of static deformations resulting from the seismic dislocation, computed through the algorithm of *Mansinha and Smylie* [1971] in the geometry of a homogeneous half-space. This approximation is appropriate as the rise time of an earthquake is always much shorter than the characteristic time needed by a tsunami wave to flush the displaced water out of the generation area [*e.g., Saito and Furumura,* 2009; *Derakhti et al.*, 2019]. For the composite mechanism of Source **S.I**, we simply superimpose the fields of deformation of the two individual subevents.

The simulation uses the 2–arcmin grid ETOPO2 [*Anonymous,* 2001], and a time step of 5 s, satisfying the CFL stability condition [*Courant et al.,* 1928]; it is carried on for 24 hours. We do not compute the interaction of the wavefield with very shallow bathymetry or initially dry land, but rather stop the computation at the 20–m isobath in the vicinity of coastlines. This procedure still allows the comparison, at a given site, of tsunamis emanating from neighboring but distant provinces.

Figures 2 and 3 show examples of the distribution of maximum amplitudes η_{max} over the Indian Basin. They constitute a classical example of the control of far-field tsunami amplitude by a combination of directivity effects, with a maximum radiation in a

direction perpendicular to the fault rupture *Ben Menahem and Rosenman*, [1972], and of focusing or defocusing effects by irregular bathymetry [*Woods and Okal*, 1987; *Satake*, 1988]. The latter is especially prominent along the Southwest Indian Ocean Ridge in the case of Sources **S.II**, **S.V**, and to a lesser extent **S.I**. The former predicts a significant change in the azimuth of maximum radiation between the 2004 source **(S.I)** which had a source curving Northwards along the Andaman arc, with the lobe of maximum radiation targeting Sri Lanka and the Maldives, and events limited to the mostly linear Sumatra Trench (**S.II**, **S.V**) whose far-field will be directed towards largely empty parts of the basin (with the exception of isolated islands such as Amsterdam or Kerguelen), but could also affect the Mascarenes and Madagascar. Similarly, the Makran scenarios shown on Figure 3 see most of their energy aimed at the Southern Indian Ocean Basin, with little if any refracted towards Africa. By contrast, the Western Coast of India is systematically illuminated by tsunami rays from the Makran sources.

3. Results and Discussion

3.1. Gauges

The locations of the 25 virtual gauges are given in Table 2 and mapped on Figure 1. In order to prevent confusion with Paper I, while at the same time maximizing continuity in the gauge dataset, we re-index them starting at 101; this also allows to distinguish locations for those gauges whose site has been moved slightly, to achieve commonality of water depths.

Figures 4 (Sumatra sources) and 5 (Makran sources) show the profiles of

maximum amplitude at the gauges, as a function of their index. The vertical gray dotted lines isolate groups of gauges whose location varies continuously with index, allowing a direct comparison of amplitude as the gauges are moved regularly along a shoreline or in an island group. As such, the dotted lines represent discontinuities in the distribution of gauges, across which the line plot has been interrupted. In the first group, and starting at low index, the gauges move continuously along the Eastern coast of Africa from Oman in the North (101) all the way to Port Elizabeth (115) in the South. The second group (116–118) is spread along the coast of Madagascar, the third one (119–122) features the four islands of the Comoro Archipelago, and the final one (123–125) the Seychelles and Mascarenes (Réunion and Rodrigues).

3.2. Results: Sumatra; Figures 2 and 4

Along the coast of East Africa, maximum amplitudes are generally contained under 20 cm (with a couple of exceptions described below), and their lateral variations limited. Remarkably, Models **S.II** and **S.V** produce amplitudes larger than the 2004 event (Model **S.I**), even though the moments of the parent earthquakes are smaller. As discussed above, this effect, which increases as the receiver moves South, expresses directivity at the source [*Ben Menahem and Rosenman*, 1972], the major lobe of radiation beaming to a Southwestern, as opposed to Western, azimuth.

This constitutes a major observation, namely that the 2004 tsunami did not amount to a "worst-case scenario", even though it led to significant casualties notably in Tanzania, where at least 12 people were confirmed dead, with reportedly more in the unsurveyed Southern part of the country [*Okal et al.*, 2009], and probably in Mozambique

where the tsunami was not surveyed. The only exception to this pattern would be Somalia (103), located in the axis of the 2004 directivity lobe, where Scenario **S.V** could be deficient and **S.II** of comparable amplitude, with respect to 2004.

Another remarkable property is that the coastlines of Mozambique are only weakly sheltered by Madagascar, and the local minimum in amplitudes observed around Moma (110; ~17º S) remains about 2/3 of the values along unobstructed coastlines to the North, such as Zanzibar (105; ~6.5º S).

Our results are particularly critical in the case of Madagascar, where all models show a regular increase in amplitude form North to South, this trend being generally confirmed by the dataset of 2004 surveyed run-up values [*Okal et al.*, 2006*a*]. In this respect, Figure 2 suggests that the Mascarene Plateau, a 1500-km continuous feature rising essentially to sea-level and linking the Seychelles to Mauritius, acts as a barrier effectively sheltering Northern Madagascar, while waves can reach its Southern coast by skirting the Mascarene Islands (Rodrigues, Mauritius and Réunion). When coupled with a favorable directivity under Scenarios **S.II** (and to a lesser extent, **S.V**), amplitudes could reach 3 to 4 times those of 2004, which resulted in run-up reaching 5.4 m at Betanty, at the extreme Southern tip of the island, and one casualty at Manafiafi, 35 km to the North [*Okal et al.*, 2006].

By contrast, the various scenarios produce only limited amplitudes off the Comoro Islands, with only marginal amplification over the 2004 values in the case of Model **S.II**. However, we recall that local run-up consistently reached 4 to 6.9 m along the Northern coast of Grande Comore [*Okal et al.*, 2009], which leaves that island at

significant risk under most future scenarios.

Finally, a more favorable directivity again leads to enhanced tsunami amplitudes in the Mascarene Islands (Réunion and Mauritius), under Scenarios **S.II** and **S.V**, where the 2004 tsunami ran up to 2.9 m. By contrast, the 2004 tsunami could constitute a worst-case scenario in the Seychelles, which clearly sit to the North of the directivity lobes of **S.II** and **S.V**. While the 1833 tsunami was observed in the Seychelles [*Jackson et al.*, 2005], those reports are not quantitative.

3.3. Results: Makran; Figures 3 and 5

With the exception of the speculative Model **M.G**, simulations for the Makran sources yield generally much smaller amplitudes at our virtual gauges than for the Sumatra models. This a combined reflection of the generally smaller size of the seismic sources, and of their orientation, which results in directivity lobes beaming SSE, away from Africa and its neighboring islands. For Makran sources, the reference event (**M.B**) consists of the well-documented, seismologically instrumented 1945 shock, whose tsunami has been both surveyed in the field [*Okal et al.*, 2015; *Anonymous*, 2015] and modeled [*e.g.*, *Heidarzadeh et al.*, 2008; *Heidarzadeh and Satake*, 2015]; note however that the 1945 earthquake triggered a significant submarine landslide, which should only marginally affect its tsunami in the far field.

As would be expected under this particular geometry, moving the source West (**M.A**) or East (**M.C**) leaves the far-field amplitude pattern essentially unchanged, while the composite sources (**M.B**, **M.E**, **M.F**) feature values enhanced by an average factor of

two, which could lead to significant run-up values in the Seychelles and Rodrigues.

Only the extreme, speculative model **M.G** produces decimetric amplitudes approaching those simulated for Sumatran sources. Their distribution along the coast of East Africa remains similar to those of smaller scenarios, with the exception of the three northernmost gauges, from Oman (101) to Somalia (103) which would be severely impacted under that scenario. Amplitudes at Gauges 101–115 would typically be 3 to 4 times those simulated under the 1945 **M.B** scenario. While the Comoros could see amplitudes enhanced to potential hazard levels comparable to those in 2004, the situation in Madagascar is not comparable to Sumatran scenarios, since it clearly sits outside the main lobe of directivity, and is further protected by the Northern branch of the Mascarene Plateau and the Seychelles, the latter featuring a large amplitude (123), which however fails to reach the level of the 2004 or 1833 Sumatran scenarios. Finally, note that Model **M.G** is the only to produce significant amplitudes in the Gulf of Aden, with possible hazard to the ports of Aden and Djibouti.

4. Conclusion

An enhanced update of our previous work in Paper I leads to the following conclusions:

- The distribution of off-shore tsunami amplitudes at a common water depth of 1000 m varies significantly with the location of mega-earthquakes along the Sumatra Trench, as a result of the combination of directivity effects and refraction by irregular bathymetry.

- Consequently, and despite its extreme moment (1.2×10^{30} dyn*cm), which may not be

duplicated in future Sumatran large earthquakes, the 2004 Sumatra-Andaman event does not always constitute the worst-case scenario for tsunami hazard at various sites on the East African shoreline or its neighbor islands. We regard this as a crucial result, since the exceptional size of the 2004 event could give a false sense of security from a disastrous basin-wide tsunami following great earthquakes which may not match its seismic moment.

- Paramount among threatened shorelines is the case of Southern Madagascar, which could expect much larger waves than in 2004 (when they already reached 5 m run-up) in a repeat of the 1833 event, for which, incidentally, we lack reliable local records.

- The whole Eastern coast of Africa would also face larger amplitudes from a source displaced South from the 2004 event, and increasingly so as the receiver is moved South, culminating in an amplification factor of about 3 with respect to the 2004 scenario, when significant damage and two casualties occurred at Port Elizabeth [*Rabinovich and Thomson*, 2007].

- In general, tsunami hazard from large events in the Makran remains relatively low, due mainly to unfavorable directivity at the source, the only potential exception being the highly improbable model **M.G**, which could occasionally give rise to amplitudes comparable to those observe in 2004. Given the continuing level of speculation surrounding the nature of the plate convergence in the Western Makran, it is clear that a program of multidisciplinary research is warranted in that region, including monitoring of sea-floor deformation through underwater geodesy, as well as paelo-tsunami investigations.

References

Ambraseys, N.N., and C.P. Melville, *A history of Persian earthquakes*, Cambridge Univ. Press., Cambridge, 219 p., 1982.

Ando, M., Source mechanism and tectonic significance of historical earthquakes along the Nankai Trough, Japan, *Tectonophysics*, **27**, 119−140, 1975.

Anonymous, ETOPO2, *Global 2 Arc-Minute Ocean Depth and Land Elevation from the US National Geophysical Data Center*, NOAA, U.S. Dept. Commerce, Washignton, DC, 2001.

Anonymous, United Nations Hyogo Declaration on Disaster Reduction, A/CONF.206/6, http://www.unhcr.org/refworld/docid/42b988b24.html, 2005,

Anonymous, *Remembering the 1945 Makran tsunami*, Intergov. Oceanog. Comm., UNESCO, Paris, 86 pp., 2015.

Ben-Menahem, A., and M. Rosenman, Amplitude patterns of tsunami waves from submarine earthquakes, *J. Geophys. Res.*, **77**, 3097−3128, 1972.

Bernard, E.N., and V.V. Titov, Evolution of tsunami warning systems and products, *Phil. Trans. R. Soc. London, Ser. A*, **373**, 20140371, 14 pp., 2015.

Borrero, J.C., R. Weiss, E.A. Okal, R. Hidayat, Suranto, D. Arcas, and V.V. Titov, The tsunami of 12 September 2007, Bengkulu Province, Sumatra, Indonesia: Post-tsunami survey and numerical modeling, *Geophys. J. Intl.*, **178**, 180−194, 2009.

Cisternas, M., B.F. Atwater, F. Torrejon, Y. Sawai, G. Machuca, M. Lagos, A. Eipert, C. Youlton, I. Salgado, T. Kamatabi, M. Shishikura, C.P. Rajendran, J.K. Malik, Y. Rizal, and M. Husni, Predecessors of the giant 1960 Chile earthquake, *Nature*, **437**, 404−407, 2005.

Courant, R., K. Friedrichs, and H. Lewy, Uber die partiellen Differenzengleichungen der mathematischen Physik, *Mathematische Annalen*, **100**, 32−74, 1928.

Derakhti, M., R.A. Dalrymple, E.A. Okal, and C.E. Synolakis, Temporal and topographic source effects in tsunami generation, *J. Geophys. Res. Oceans*, **124**, 5270−5288, 2019.

Fritz, H.M., and J.C. Borrero, Somalia Field Survey after the December 2004 Indian Ocean Tsunami, *Earthquake Spectra*, **22**, S219−S233, 2006.

Fritz, H.M., and E.A. Okal, Socotra Island, Yemen: Field survey of the 2004 Indian Ocean tsunami, *Natural Hazards*, **46**, 107−117, 2008.

Godunov, S.K., Finite difference methods for numerical computations of discontinuous solutions of the equations of fluid dynamics, *Matemat. Sbornik*, **47**, 271−295, 1959.

Heidarzadeh, M., and K. Satake, New insights into the source of the Makran tsunami of 27 November 1945 from tsunami waveforms and coastal deformation data, *Pure Appl Geophys.*, **172**, 621−640, 2015.

Heidarzadeh, M., M.D. Pirooza, N.H. Zakerb, A.C. Yalcıner, M. Mokhtari, and A. Esmaeilye, Historical tsunami in the Makran Subduction Zone off the southern coasts of Iran and Pakistan and results of numerical modeling, *Ocean Eng*., **35**, 774−786, 2008.

Jackson, L.E., J.V. Barrie, D.L. Forbes, J. Shaw, G.K. Mawson, and M. Schmidt, Effects of the 26 December 2004 Indian Ocean tsunami in the Republic of Seychelles, *Eos Trans. Amer. Geophys. Un.*, **86**, (52), F6−F7, 2005 [abstract].

Kelsey, H.M., A.R. Nelson, E. Hemphill-Haley, and R.C. Witter, Tsunami history of an Oregon coastal lake reveals a 4600-yr record for great earthquakes on the Cascadia

subduction zone, *Geol. Soc. Amer. Bull.*, **117**, 1009−1032, 2005.

Kukowski, N., T. Schillhorn, E.R. Flueh, and K. Hurn, Newly identified strike-slip plate boundary in the Northeastern Arabian Sea, *Geology*, **28**, 355−358, 2000.

Mansinha, L., and D.E. Smylie, The displacement fields of inclined faults, *Bull. Seismol. Soc. Amer.*, **61**, 1433−1440, 1971.

McCloskey, J., D. Lange, F. Tilmann, S.S. Nalbant, A.F. Bell, D.H. Natawidjaja, and A. Rietbock, The September 22009, Padang earthquake, *Nature Geosc.*, **3**, 70−71, 2010.

Mokhtari, M., I.A. Fard, and Kh. Hessami, Structural elements of the Makran region, Oman Sea and their potential relevance to tsunamigenisis, *Natural Haz.,* **47**, 185−199, 2008.

Musson, R.M.W., Subduction in the Western Makran: the historian's contribution, *J. Geol. Soc. London*, **166**, 387−391, 2009.

Nanayama, F., K. Stake, R. Furukawa, K. Shimokawa, B.F. Atwater, K. Shigeno, and S. Yamaki, Unusually large earthquakes inferred from tsunami deposits along the Kuril trench, *Nature*, **424**, 660−663, 2003.

Natawidjaja, D.H., K. Sieh, M. Chlieh, J. Galetzka, B. Suwargadi, H. Cheng, R.L. Edwards, J.-P. Avouac, and S. Ward, Source parameters of the great Sumatran earthquakes of 1797 and 1833 inferred from coral microatolls, *J. Geophys. Res.*, **111**, (B6), B06403, 37 pp., 2006.

Okal, E.A., and C.E. Synolakis, Far-field tsunami hazard from mega-thrust earthquakes in the Indian Ocean, *Geophys. J. Intl.*, **172**, 995−1015, 2008.

Okal, E.A., H.M. Fritz, R. Raveloson, G. Joelson, P. Pančošková, and G. Rambolamanana, Madagascar field survey after the December 2004 Indian Ocean tsunami, *Earthquake Spectra*, **22**, S263−S283, 2006a.

Okal, E.A., H.M. Fritz, P.E. Raad, C.E. Synolakis, Y. Al-Shijbi, and M. Al-Saifi, Oman field survey after the December 2004 Indian Ocean tsunami, *Earthquake Spectra*, **22**, S203−S218, 2006b.

Okal, E.A., A. Sladen, and E.A.-S. Okal, Rodrigues, Mauritius and Reunion Islands field survey after the December 2004 Indian Ocean tsunami, *Earthquake Spectra*, **22**, S241−S261, 2006c.

Okal, E.A., H.M. Fritz, and A. Sladen, 2004 Sumatra tsunami surveys in the Comoro Islands and Tanzania and regional tsunami hazard from future Sumatra events, *South Afr. J. Geol.*, **112**, 343−358, 2009.

Okal, E.A., H.M. Fritz, M.A. Hamzeh, and J. Ghasemzadeh, Field survey of the 1945 Makran and 2004 Indian Ocean tsunamis in Baluchistan, Iran, *Pure Appl. Geophys.*, **172**, 3343−3356, 2015.

Pendse, C.G., The Mekran earthquake of the 28th November 1945, *India Meteorol. Dept. Sci. Notes*, **10**, 141−146, 1946.

Rabinovich, A.B., and R.E. Thomson, The 26 December 2004 Sumatra tsunami: Analysis of tide gauge data from the world ocean; Part 1. Indian Ocean and South Africa, *Pure Appl. Geophys.*, **164**, 261−308, 2007.

Rajendran, C.P., K. Rajendran, M. Shah-Hosseini, A.Naderi-Beni, C.M. Nautiyal, and R. Andrews, The hazard potential of the western segment of the Makran subduction zone, northern Arabian Sea, *Natural Haz.*, **65**, 219−239, 2013.

Reymond, D., and E.A. Okal, Preliminary determination of focal mechanisms from the inversion of spectral amplitudes of mantle waves, *Phys. Earth Planet. Inter.*, **121**, 249−271, 2000.

Saito, T., and T. Furumura, Three-dimensional tsunami generation simulation due to sea-bottom deformation and its interpretation based on the linear theory, *Geophys. J. Intl.*, **178**, 877−888, 2009.

Satake, K., Effects of bathymetry on tsunami propagation: Application of ray tracing to tsunamis, *Pure Appl. Geophys.*, **126**, 27−36, 1988.

Synolakis, C.E., Tsunami and seiche, **in:** *Earthquake Engineering Handbook*, ed. by W.-F. Chen and C. Scawthron, pp. **9**_1−**9**_90, CRC Press, Boca Raton, 2003.

Synolakis, C., E. Bernard, V. Titov, U. Kanoglu, and F. Gonzalez, Validation and verification of tsunami numerical models, *Pure Appl. Geophys.*, **165**, 2197−2228, 2008.

Titov, V.V., and C.E. Synolakis, Numerical modeling of tidal wave runup, *J. Waterway, Port, Coast. Oc. Eng*., **124**, 157−171, 1998.

Titov, V., U. Kanoglu, and C. Synolakis, Development of MOST for real-time tsunami forecasting, *J. Waterway Port Coast Oc. Eng.,* **142**, (6), 03116004, 16 pp., 2016.

Weiss, R., and H. Bahlburg, The coast of Kenya field survey after the December 2004 Indian Ocean tsunami, *Earthquake Spectra*, **22**, S235−S240, 2006.

White, R.S. and K. Klitgord, Sediment deformation and plate tectonics in the Gulf of Oman, *Earth Planet. Sci. Letts.*, **32**, 199−209, 1976.

Woods, M.T., and E.A. Okal, Effect of variable bathymetry on the amplitude of teleseismic tsunamis: a ray-tracing experiment, *Geophys. Res. Letts.*, **14**, 765-768, 1987.

Zachariasen J., K. Sieh, F.W. Taylor, R.L. Edwards, and W.S. Hantoro, Submergence and uplift associated with the giant 1833 Sumatran subduction earthquake: Evidence from coral microatolls, *J. Geophys. Res.,* **104**, 895−919, 1999.

Figure Captions

Figure 1.: Map of the 25 virtual gauges used in this study. The numbers are keyed the indices listed in Table 1. The inset zooms on the Comoro Archipelago shown as the gray box on the main map.

Figure 2.: Examples of basin-wide simulations in the case of Sumatra sources. Model **S.I** reproduces the 2004 Sumatra-Andaman event; Scenario **S.II** is a model the 1833 tsunami; Scenario **S.IV** is a possible model of a future earthquake closing the Padang seismic gap; and Scenario **S.V** includes a speculative rupture along the Southern part of the Sumatra Trench.

Figure 3.: Same as Figure 2 for a selection of Makran simulations. Scenario **M.A** is a possible model of the 1851 event; Scenario **M.B** is a model the 1945 tsunami; Scenario **M.D** is a combination of A and B; and Scenario **M.F** of the three blocks A, B, and C.

Figure 4.: Summary of Sumatra simulations at the 25 virtual gauges. *(a):* Maximum absolute amplitude recorded at each gauge, color-coded according to source model (see Table 1). *(b):* Amplitudes relative to 2004, plotted on a logarithmic scale. See text for discussion.

Figure 5.: Same as Figure 4 in the case of the Makran simulations. Note the different vertical scale in (a). In (b), amplitudes are taken relative to the quantified event of 1945.

TABLE 1. Parameters of the sources used in the numerical simulations.

Number	Source	Centroid		Fault parameters			Moment	Focal Mechanism		
		(°N)	(°E)	Length L (km)	Width W (km)	Slip Δu (m)	(10^{29} dyn*cm)	ϕ (°)	δ (°)	λ (°)
					Sumatra Sources					
S.I.a	2004,a	3.3	94.6	382	150	11.5	3.2	318	6.4	94
S.I.b	2004,b	7.0	93.8	818	150	12.4	7.3	355	7	109
S.I	Sumatra-Andaman 2004			1200	150		10.5			
S.II	Mentawai 1833	-3.0	99.7	550	175	13	6.0	322	12	90
S.III	Bengkulu	-4.4	101.6	190	95	5.6	0.5	329	8	100
S.IV	1833 post-2007	-3.7	100.6	350	175	6.0	1.9	322	12	90
S.V	IV + South	-4.25	100.7	900	175	8.0	6.0	322	12	90
					Makran Sources					
M.A	1851	24.85	62.1	157	78	4.62	0.28	281	9	89
M.B	1945	24.855	63.545	157	78	4.62	0.28	261	9	89
M.C	1765	25.1	65.1	157	78	4.62	0.28	261	9	89
M.D	A+B						0.56			
M.E	B+C						0.56			
M.F	A+B+C						0.84			
M.G	F + West						4.70			

TABLE 2. Location of virtual gauges used in this study.

Index		Latitude	Longitude	Location	Country
This Study	Paper I	(°N)	(°S)		
101	1	17.475	56.500	Hallaniyah Is.	Oman
102	2	12.270	54.610	Socotra Is.	Yemen
103	3	9.100	51.205	Bandarbeyla	Somalia
104	5	-3.980	40.620	Mombasa	Kenya
105	6	-6.520	39.792	Zanzibar Is.	Tanzania
106		-10.440	40.745	Rovuma River	Tanzania/Mozambique
107		-10.790	40.863	Palma	Mozambique
108		-12.920	40.707	Pemba	Mozambique
109		-15.140	40.913	Nampula Province	Mozambique
110		-16.960	39.884	Moma	Mozambique
111		-19.000	37.380	Zambeze River	Mozambique
112	16	-19.960	36.620	Beira	Mozambique
113	17	-26.600	34.256	Maputo	Mozambique
114	18	-30.160	31.650	Durban	South Africa
115	19	-34.109	27.000	Port Elizabeth	South Africa
116	11	-15.030	50.551	Antalaha	Madagascar (N)
117	12	-19.597	49.192	Mahanoro	Madagascar (C)
118	13	-23.991	47.700	Manantehina	Madagascar (S)
119	7	-11.450	43.555	Grande Comore	Comoros
120	8	-12.214	43.851	Moheli	Comoros
121	9	-12.048	44.510	Anjouan	Comoros
122	10	-12.560	45.233	Koungou, Mayotte	France
123	4	-4.490	56.451	Mahé Is.	Seychelles
124	15	-20.814	55.521	Saint-Denis, Réunion	France
125	14	-19.640	63.590	Rodrigues	Mauritius

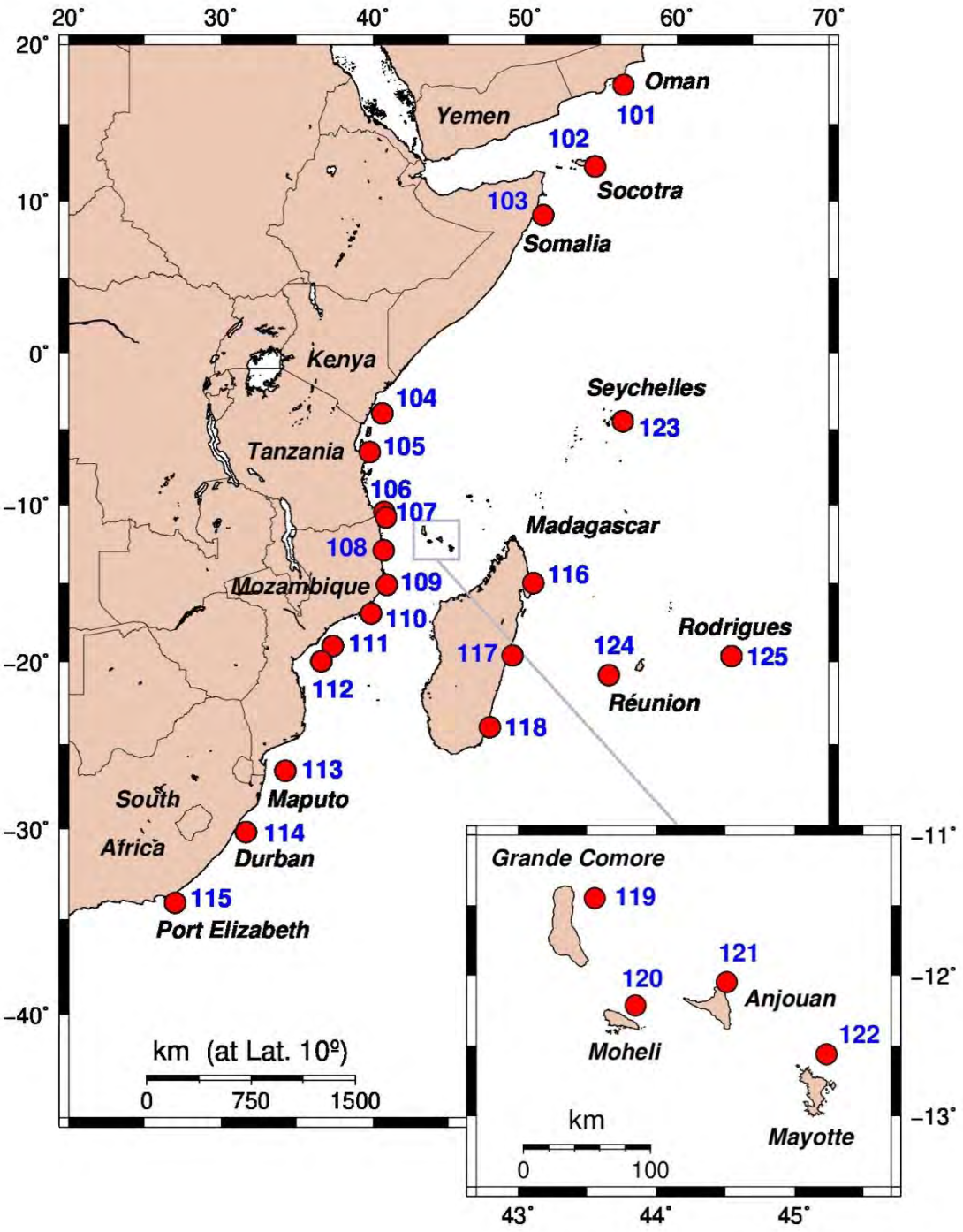

Figure 1.: Map of the 25 virtual gauges used in this study. The numbers are keyed the indices listed in Table 1. The inset zooms on the Comoro Archipelago shown as the gray box on the main map.

Figure 2.: Examples of basin-wide simulations in the case of Sumatra sources. Model **S.I** reproduces the 2004 Sumatra-Andaman event; Scenario **S.II** is a model the 1833 tsunami; Scenario **S.IV** is a possible model of a future earthquake closing the Padang seismic gap; and Scenario **S.V** includes a speculative rupture along the Southern part of the Sumatra Trench.

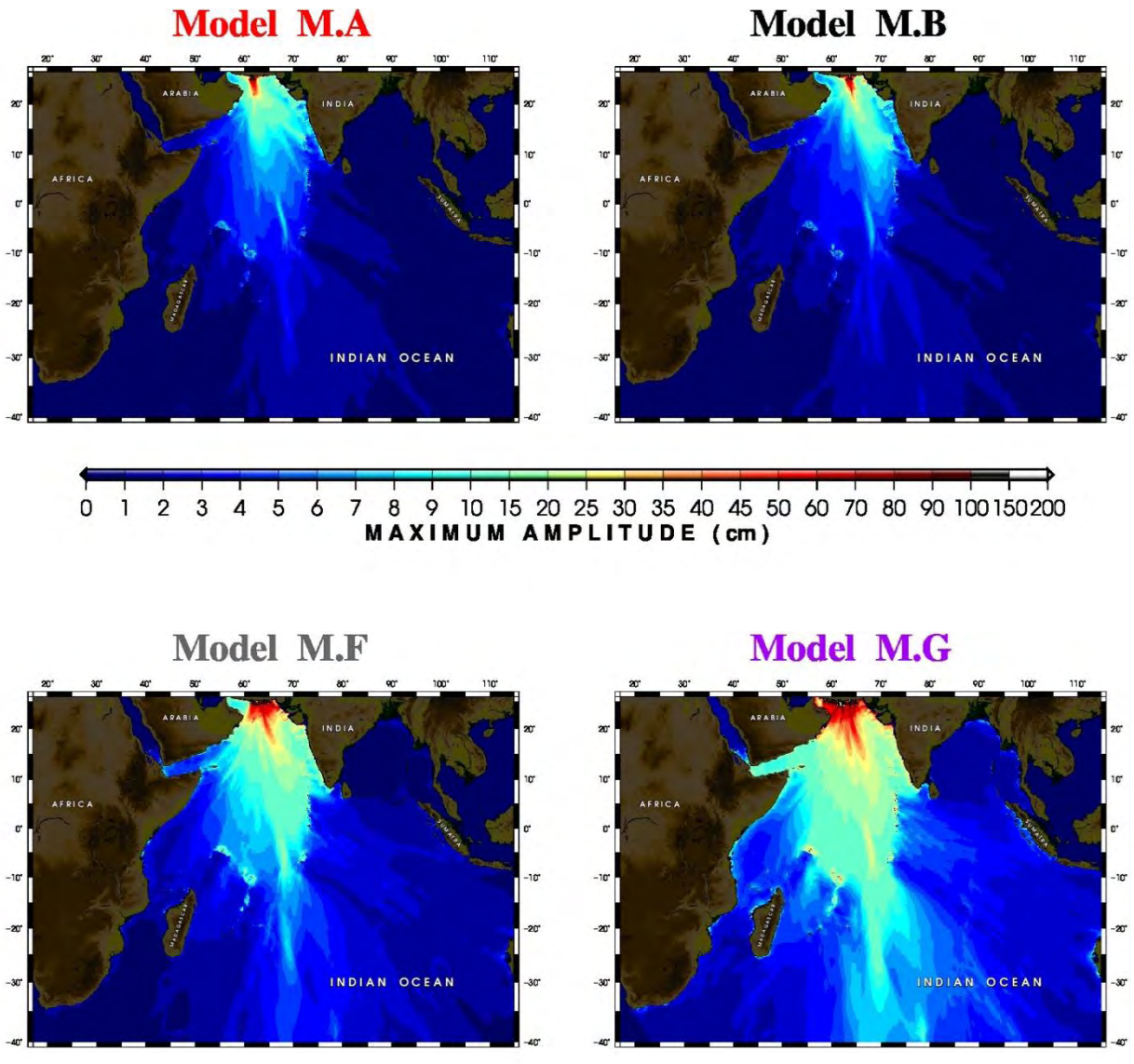

Figure 3.: Same as Figure 2 for a selection of Makran simulations. Scenario **M.A** is a possible model of the 1851 event; Scenario **M.B** is a model the 1945 tsunami; Scenario **M.D** is a combination of A and B; and Scenario **M.F** of the three blocks A, B, and C.

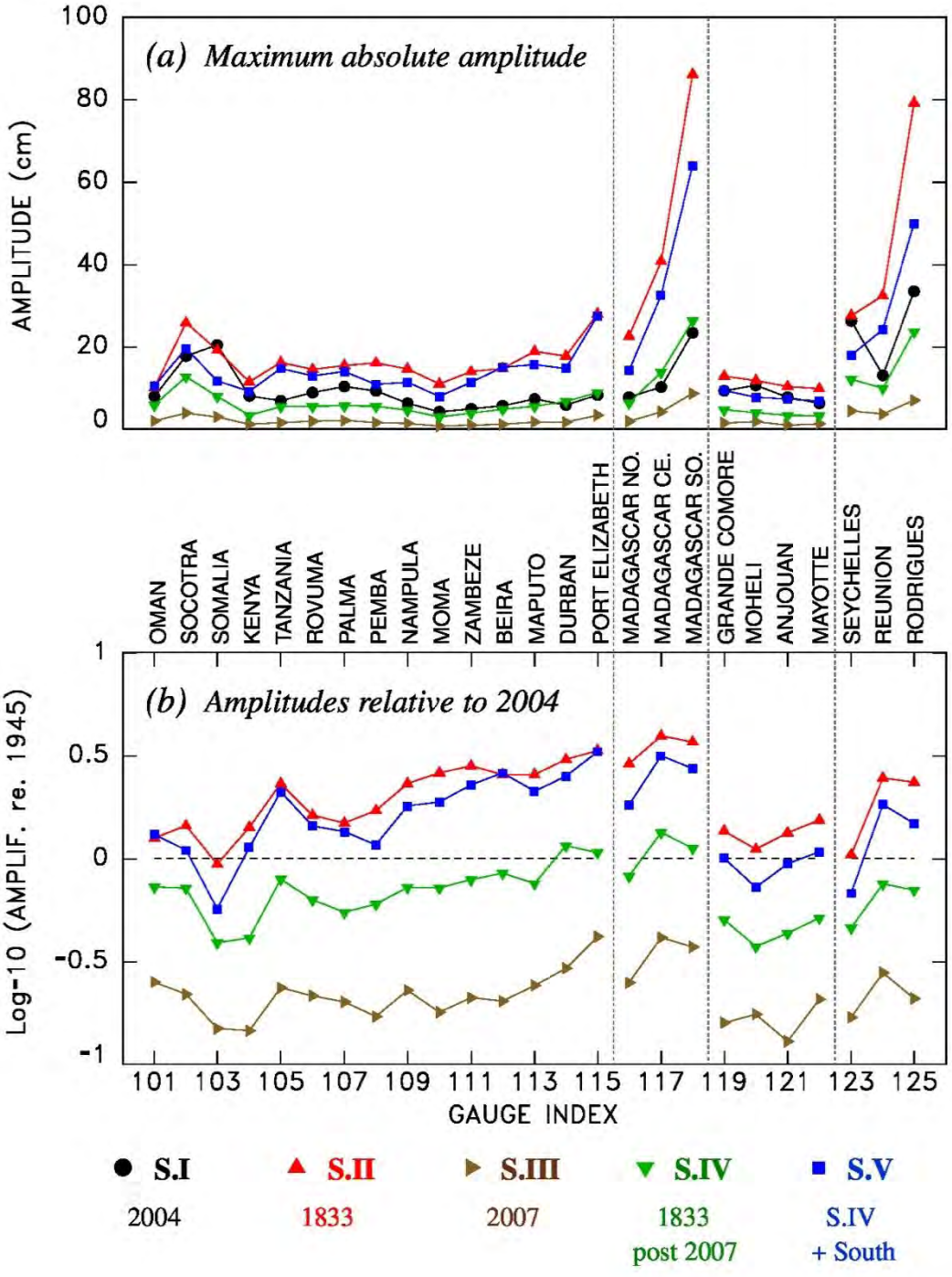

Figure 4.: Summary of Sumatra simulations at the 25 virtual gauges. *(a):* Maximum absolute amplitude recorded at each gauge, color-coded according to source model (see Table 1). *(b):* Amplitudes relative to 2004, plotted on a logarithmic scale. See text for discussion.

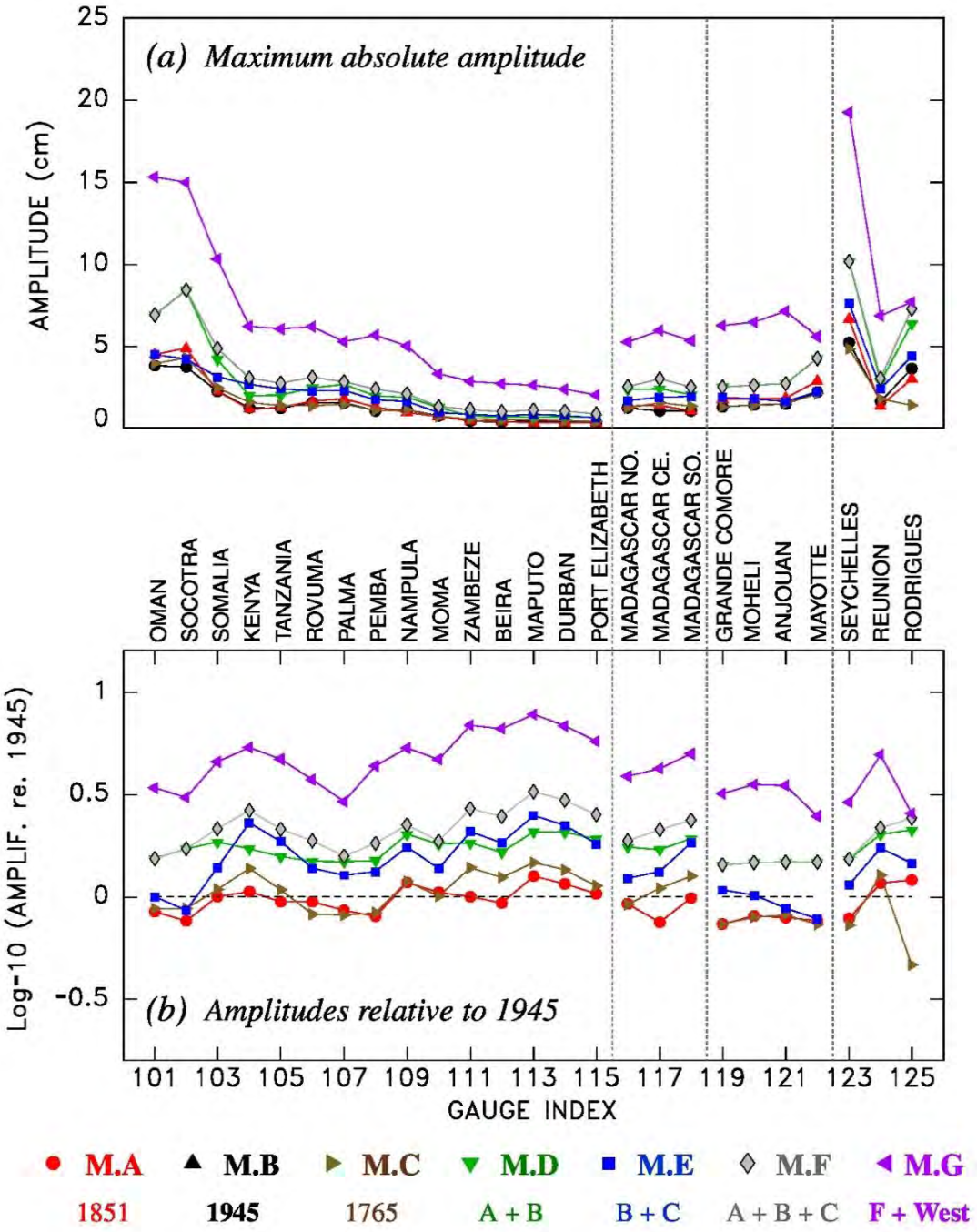

Figure 5.: Same as Figure 4 in the case of the Makran simulations. Note the different vertical